# Visualizing the three-dimensional arrangement of hydrogen atoms in organic molecules by Coulomb explosion imaging

Alice E. Green,[1,2,3,*] Keyu Chen,[4,†] Surjendu Bhattacharyya,[4,1] Felix Allum,[1,5] Sergey Usenko,[2] Michael N. R. Ashfold,[6] Thomas M. Baumann,[2] Kurtis D. Borne,[4,1] Mark Brouard,[7] Michael Burt,[7] Basile F. E. Curchod,[6] Benjamin Erk,[5] Ruaridh J. G. Forbes,[1] Lea M. Ibele,[8] Rebecca A. Ingle,[9] Huynh Van Sa Lam,[4] Xiang Li,[1] Kang Lin,[10] Tommaso Mazza,[2] Joseph W. McManus,[7] Michael Meyer,[2] Terrence Mullins,[2] Joao Pedro Figueira Nunes,[11] Daniel Rivas,[2] Aljoscha Roerig,[2] Arnaud Rouzée,[12] Philipp Schmidt,[2] John Searles,[4] Björn Senfftleben,[2] Henrik Stapelfeldt,[13] Rico Mayro P. Tanyag,[13] Florian Trinter,[14] Anbu Selvam Venkatachalam,[4] Enliang Wang,[4] Emily M. Warne,[7] Peter M. Weber,[15] Thomas J. A. Wolf,[1] Till Jahnke,[2,16] Artem Rudenko,[4] Rebecca Boll,[2,‡] and Daniel Rolles[4,§]

[1] *SLAC National Accelerator Laboratory, Menlo Park, California 94025, USA*
[2] *European XFEL, Holzkoppel 4, 22869 Schenefeld, Germany*
[3] *EaStCHEM School of Chemistry, University of Edinburgh, Edinburgh EH9 3FJ, United Kingdom*
[4] *James R. Macdonald Laboratory, Physics Department, Kansas State University, Manhattan, KS 66506, USA*
[5] *Deutsches Elektronen-Synchrotron DESY, Notkestrasse 85, 22607 Hamburg, Germany*
[6] *School of Chemistry, Cantock's Close, University of Bristol, Bristol, BS8 1TS, UK*
[7] *Chemistry Research Laboratory, Department of Chemistry, University of Oxford, Oxford OX1 3TA, UK*
[8] *Aix Marseille University, CNRS, ICR, 13397 Marseille, France*
[9] *Department of Chemistry, University College London, London, WC1H 0AJ, UK*
[10] *Institut für Kernphysik, Goethe-Universität Frankfurt, Max-von-Laue-Str. 1, 60438 Frankfurt am Main, Germany*
[11] *Diamond Light Source Ltd, Didcot, OX11 0DE, UK*
[12] *Max-Born-Institut, Max Born Straße 2A, 12489 Berlin, Germany*
[13] *Department of Chemistry, Aarhus University, Langelandsgade 140, DK-8000 Aarhus C, Denmark*
[14] *Molecular Physics, Fritz-Haber-Institut der Max-Planck-Gesellschaft, Faradayweg 4-6, 14195 Berlin, Germany*
[15] *Department of Chemistry, Brown University, Providence, RI, USA*
[16] *Max-Planck-Institut für Kernphysik, 69117 Heidelberg, Germany*

(Dated: August 15, 2025)

Structure-sensitive methods based on femtosecond light or electron pulses are now making it possible to measure how molecular structures change during light-induced processes. Despite significant progress, high-fidelity imaging of nuclear positions remains a challenge even for relatively small molecular systems and, notably, regarding the positions of hydrogen atoms. As demonstrated in recent work, X-ray induced Coulomb explosion imaging (CEI) may overcome this obstacle as its sensitivity does not depend on the mass of the imaged atoms. The photoinduced ring opening of the heterocyclic molecule 2(5H)-thiophenone has attracted recent interest. Here, we show that CEI offers a powerful route to imaging the peripheral H atoms in this molecule and thus, more generally, to tracking detailed nuclear motions (e.g. isomerizations) in organic molecules on ultrafast timescales. Specifically, we record momentum-space Coulomb explosion images that report on the three-dimensional positioning of all nuclei within the molecule, for instance distinguishing H atoms in C–H bonds that lie within or are directed out of the plane defined by the heavy atoms. The prospect of imaging peripheral H atoms to probe photochemical dynamics is explored by coupling ab initio molecular dynamics with classical Coulomb explosion simulations and thereby differentiating potential photoproduct isomers, including those whose structures primarily differ in the position of the hydrogens.

Keywords: photochemistry, ultrafast imaging, femtosecond, X-ray free-electron laser, Coulomb explosion imaging

## INTRODUCTION

A number of state-of-the-art structural imaging techniques exist that can operate on ultrafast (femtosecond) timescales. Such approaches, which include diffractive imaging by intense electron [1, 2] or X-ray [3, 4] pulses, offer routes to investigating ultrafast photochemistry of gas-phase molecules, but they are also subject to some restrictions: relatively high sample densities

* alice.green@ed.ac.uk
† both authors (Green and Chen) have contributed equally to this work
‡ rebecca.boll@xfel.eu
§ rolles@ksu.edu

are required, the sensitivity to light atoms (particularly H atoms, which have small scattering cross sections) is low, and structural information is typically averaged over an isotropic, randomly oriented sample ensemble [4]. Coulomb explosion imaging (CEI) promises to overcome these challenges. It offers much higher sensitivity, such that dilute samples can be studied, including low vapor pressure samples [5, 6], (mass-selected) weakly bound clusters [7–9], rotationally cold molecules in supersonic beams (which may be state-selected [10] and/or aligned [11, 12]), and molecules and clusters embedded in helium nanodroplets [13, 14]. Crucially, the high sensitivity applies to all atoms within a molecule, including H atoms, equally. Furthermore, through coincidence analysis, information can be extracted within a molecular frame, even for a randomly oriented sample [5, 6, 15–21]. Consequently, the structural insights can extend far beyond average pair distances, which determine (angle-averaged) scattering patterns, to information pertaining to bond angles [6, 22–24] and, ideally, the identification of different three-dimensional (3D) conformations [16, 25]. The latter is broadly applicable to the study of chemical structures and dynamics. For example, organic molecules often exist in multiple structural isomers in which the H atoms may have different 3D arrangements. Different isomers can exhibit distinctly different chemical function, but are difficult to distinguish on ultrafast timescales, especially in the gas phase. Developing techniques which can visualize the position and motion of individual H atoms in isolated gas-phase molecules on femtosecond timescales is thus of great potential importance. Recent work has shown sensitivity to ultrafast hydrogen motion in (deuterated) ammonia using ultrafast electron and X-ray diffraction methods [26–28], but extending such studies to more complex molecules is extremely challenging as the relative scattering contribution of hydrogen atoms becomes prohibitively small. Here, we demonstrate that CEI induced by femtosecond X-ray pulses is a promising approach for three-dimensional imaging of individual hydrogen atoms on ultrafast timescales in relatively complex organic molecules.

The full realization of CEI relies upon a swift stripping of many electrons from a molecule, causing a prompt fragmentation into atomic ions. From the relative momenta of these ions, information about the structure prior to the explosion can be obtained. First demonstrations of static CEI were realized through collisions between accelerated monocations and a thin metal foil, thereby stripping off (valence) electrons [29]. Recent work has demonstrated the ability to image the static structure of 10-atom heterocycle molecules by inducing Coulomb explosion through collision with a high-energy, multiply charged incident atomic cation [30]. Multiple ionization is more commonly initiated with intense laser pulses [31], and state-of-the-art experiments have demonstrated that molecules of similar size can be imaged in momentum space with high quality in both two [19] and three dimensions [32]. Coupled to a suitable prior photoexcitation (henceforth pump) pulse, this naturally allows the technique to be extended to time-resolved studies [33, 34]. Such pump - CEI-probe methods have been used to study coherent rotational [35] and vibrational [23, 36, 37] motion, as well as ultraviolet (UV)-induced photochemical processes, such as photodissociations [24, 38–41] and photoisomerizations [42, 43]. However, it should be emphasized that such work has either focused on small (few-atom), structurally simple systems [24, 34–37] and/or has employed incomplete Coulomb explosion which yields larger molecular fragments [23, 38–40].

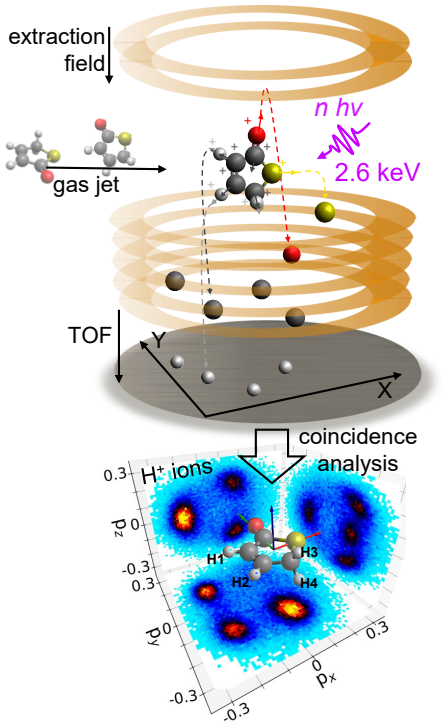


FIG. 1. Schematic overview of the experiment, showing the Coulomb explosion of thiophenone ($C_4H_4OS$; yellow: sulfur; red: oxygen; dark gray: carbon; light gray: hydrogen) molecules induced by an intense femtosecond X-ray pulse. From the three-dimensional momenta of sets of ions detected in coincidence, data can be transformed into a molecular frame, as shown in the bottom panel.

Initiating Coulomb explosion with intense X-ray pulses, as opposed to employing strong near-infrared laser pulses, promises to extend the scope of such studies [5, 18, 20, 21, 24, 44–49]. Rapid multiple core ionization and Auger-Meitner decays efficiently populate the high charge states required for complete Coulomb explosion into the constituent atomic ions, even in larger molecules. Recent work demonstrated the efficacy of Coulomb explosion for comparatively complex molecules such as 2-iodopyridine and 2-iodopyrazine with an intense X-ray free-electron laser (XFEL) source [5]. Coincident ion momentum distributions yielded momentum-space maps of the studied molecules with clear resemblance to the

known molecular structures prior to ionization and fragmentation. The approach has since been extended to measure the temporal evolution of the structure of UV-excited 2-thiouracil molecules during internal conversion, by tracing changes in the momentum-space images of its peripheral H atoms [21].

The previously mentioned aromatic molecules all have planar equilibrium geometries. Here, the concept is extended to determine whether measuring the momenta of $H^+$ ions can be used to provide 3D structural information for broader classes of organic molecules. Specifically, we report the results of an X-ray-induced CEI study of gas-phase 2(5H)-thiophenone ($C_4H_4OS$, henceforth simply termed thiophenone, the structure of which is shown in Fig. 1). The heavy atoms in this molecule lie in a common plane, but the H atom coordinates span three dimensions, with two lying in and two out of the heavy atom plane. Thiophenone is also of interest due to its rich UV photochemistry; its photoinduced ring-opening has been the subject of several recent time-resolved studies [50–52]. All four H atoms can be clearly distinguished in the recorded coincident 3D ion momentum distributions (see Fig. 1 bottom and Fig. 2 middle row). Since H atoms are usually located on the outside (i.e. on the periphery) of isolated organic molecules, the $H^+$ ions can serve as powerful reporters of the overall molecular geometry. Their light mass (and thus fast recoil) ensures that they tend to be ejected along the axis of the C–H bond from which they originate – so called 'axial' recoil. For completeness, we note that some previous CEI experiments have reported $H^+$ ion detection and investigated dynamical processes such as hydrogen migration in small molecules [53–56]. However, the 3D structural information obtained in these cases was typically more limited, either because incomplete Coulomb explosion channels were investigated or because the study was limited to planar systems [31, 32, 48, 57]. We also note examples of CEI studies involving substituted methanes, wherein 3D structural signatures of H atoms were observed [16, 20, 58].

The present experimental CEI data for ground-state thiophenone molecules are also compared with predictions based on classical Coulomb explosion simulations for (i) ground-state thiophenone molecules and (ii) various of the vibrationally excited photoproducts (e.g. ring-opened isomers and internally 'hot' thiophenone molecules) formed by internal conversion following UV photoexcitation of thiophenone returned by complementary *ab initio* molecular dynamics (AIMD) calculations. These comparisons clearly illustrate the potential of X-ray-induced CEI for tracking the photoinduced evolution of organic molecular structures, including the three-dimensional movement of H atoms.

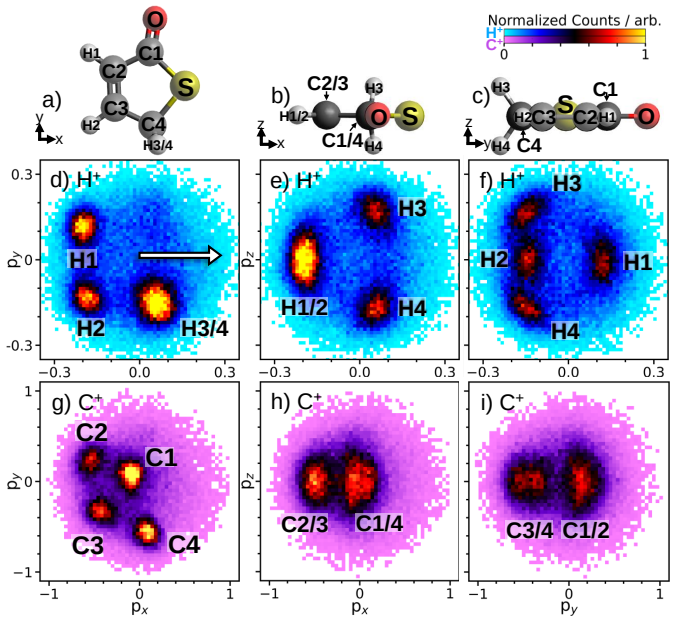


FIG. 2. Newton plots of the coincident momentum distributions of d)-f) $H^+$ and g)-i) $C^+$ ions projected onto the $xy$, $xz$ and $yz$ planes, showing the relative momenta following Coulomb explosion of thiophenone in three dimensions. Ball-and-stick models of thiophenone viewed along three orthogonal axes are displayed in panels a) to c). The counts for $H^+$ and $C^+$ are normalized independently, and are plotted on distinct color scales. As described in the text, the coordinate frame is chosen such that the $S^+$ momentum points along the positive $x$ axis (see arrow in panel d) and the $O^+$ momentum spans the $xy$ plane (with $p_y > 0$). The third particle ($H^+$ or $C^+$) is plotted within this frame and normalized to the momentum of the $S^+$ ion. Similar plots for the $O^+$ and $S^+$ ions are displayed in Fig. S2 of the SI.

## RESULTS

The experiment was carried out using the Cold Target Recoil Ion Momentum Spectroscopy (COLTRIMS) reaction microscope (REMI) of the Small Quantum Systems (SQS) scientific instrument at the European XFEL [59], depicted schematically in Fig. 1. Experimental details are given in the Methods section. Data were acquired under a sufficiently low count rate such that ions detected in the same laser shot can generally be assumed to originate from Coulomb explosion of the same thiophenone molecule. Figure 2 presents the recorded $H^+$ and $C^+$ ion momentum distributions of thiophenone in a molecular frame of reference, which distinctly show signal originating from each hydrogen and carbon atom in the molecule. There are many ways in which these correlated momentum distributions can be represented. Here, we chose a molecular frame defined as follows (and explained schematically in Fig. S1 of the Supplementary Information [SI]): the positive $x$ axis is defined along the $S^+$ momentum, while the plane spanned by the $S^+$ and $O^+$ momenta defines the $xy$ plane, with the $O^+$ fixed to have a

positive $y$ momentum component. The laboratory-frame momentum of each ion is then transformed on a shot-by-shot (i.e., molecule-by-molecule) basis into this molecular frame of reference after normalizing its magnitude by the absolute momentum of the $S^+$ ion (and after applying certain momentum filters, see 'Data Processing'). To aid with the visualization of the coordinate transform, the nuclear structure of thiophenone is displayed above the momentum distributions in Fig. 2. Coincident detection of all ten atomic ions from complete Coulomb explosion of the thiophenone molecule is extremely rare due to a typical ion detection efficiency of around 60% (which results in an overall detection efficiency for a 10-ion coincidence of, at most, $0.6^{10} = 0.6\%$). However, the Coulomb explosion image of all 10 ions can be built up from four-fold coincidence events, in which $H^+$ and/or $C^+$ ion(s) are detected in coincidence (i.e., in the same laser shot) with an $O^+$ and $S^+$ ion. This is possible if all Coulomb explosion events proceed sufficiently similarly such that ten-fold coincidences are not required to isolate the individual atoms [5]. Figure 2 focuses on the coincident $H^+$ and $C^+$ ion momenta, while the SI shows momentum distributions for all coincident ions ($H^+$, $C^+$, $O^+$, $S^+$), both with (Fig. S2) and without (Fig. S3) normalization by the $S^+$ momentum. Figure S4 presents the same data in an alternative frame in which the $O^+$ momentum, rather than the $S^+$ momentum, defines the $x$ axis. The correlation between the coincident momentum distributions and the nuclear structure prior to Coulomb explosion is striking, with the exception of C1, which gets trapped within the surrounding charges and thus emerges with lower momentum.

Turning first to the $H^+$ momentum distributions presented in Figs. 2d-2f, in the $xy$ projection (Fig. 2d), three well-localized features are seen, originating from the hydrogen atoms bonded to carbon atoms C2, C3, and C4 in the labeled molecular structure. The latter feature is more intense, as it originates from two hydrogen atoms (H3/4), lying above and below the S, O (and C) atom plane. This can be seen in the corresponding $xz$ and $yz$ projections (Figs. 2e and Fig. 2f), where H3 and H4 are cleanly separated into distinct features. The low-intensity, mostly isotropic background seen across all projections is due to 'false' coincidences, arising from the possibility of coincident detection of ions produced from different molecules. If desired, the expected contributions from such false coincidences could be subtracted off, as is routinely implemented, e.g., in covariance and cumulant mapping [22, 60–64], but is unnecessary for the present analysis.

The $C^+$ momentum distributions (Figs. 2g-2i) do not reflect the molecular structure as directly as the $H^+$ ions do. The most structurally revealing information is in the $xy$ plane (Fig. 2g), due to the heavy atoms all lying in this plane in thiophenone. In this projection, each carbon atom can be distinguished and their location in the ring determined. We direct attention to the feature arising from the C1 atom, which exhibits a much lower momentum than the other $C^+$ ions (i.e., its feature lies closer to the origin in this projected two-dimensional momentum histogram). As reproduced by classical simulations (see Fig. S8 in the SI and details of the simulation given in the Methods section), this is due to the dynamics of the Coulomb explosion itself. In the explosion, this carbon ion is 'trapped' between the $O^+$ and $S^+$ ions and the other $C^+$ ions. The simultaneous Coulomb repulsions from differing directions lead to a lower final absolute momentum, while the other carbon ions are pushed away from all other heavy ions. Similar trapping effects have been observed previously [5, 49, 65]. They are one example of many of the complex (and sometimes unintuitive) relationships between final ion momenta following Coulomb explosion and the initial structure before explosion [66, 67], emphasizing that recorded angles in momentum space do not necessarily bear similarity to the various interbond angles in the neutral parent species prior to Coulomb explosion. Therefore, real-space structure retrieval from momentum-space Coulomb explosion imaging data typically requires complementary modeling of the Coulomb explosion process [20]. This also highlights a key benefit of the use of hydrogen atoms to determine (ultrafast changes in) 3D structure. Hydrogen atoms generally lie on the periphery of a molecule and thus are less susceptible to such 'trapping' effects. Their positions thus map more faithfully onto final momenta. Furthermore, the low mass of hydrogen ensures its swift ejection from the polycation in the early stages of the Coulomb explosion before significant structural deformation occurs.

To further explore the extent of the structural information contained in the present data, we now explore alternative ways of representing the coincident 3D momentum distributions. Generally speaking, different representations can highlight specific aspects of the Coulomb explosion dynamics captured in these correlated momentum distributions, and underpin different structural features. Figures 3a and 3b show 3D isosurfaces of the experimental ion momentum distributions of the $H^+$ and $C^+$ ions, respectively. The displayed isosurfaces are color coded by the magnitude of the momenta of each ion. For both $H^+$ and $C^+$ ions, this representation allows for the islands associated with each atom in Fig. 2 to be very clearly separated and fully represented in three dimensions, whilst avoiding the difficulties in visualizing the full 3D histogram (see also Fig. S5). This representation also highlights the increased spread in out-of-plane ($p_z$) momentum for the low-momentum (purple) $C^+$ ions originating from the C1 atom, which could be less clearly observed in Figs. 2 h) and i). Classical Coulomb explosion simulations of cold thiophenone (see Fig. S10 in the SI) reproduce this observation, whereas the sampled Wigner distribution of structures used in the simulation shows no significant differences in the $z$ position of this carbon. This suggests that the larger momentum spread arises because the final $p_z$ of these $C1^+$ ions exhibits a higher sensitivity to small deviations in the initial molec-

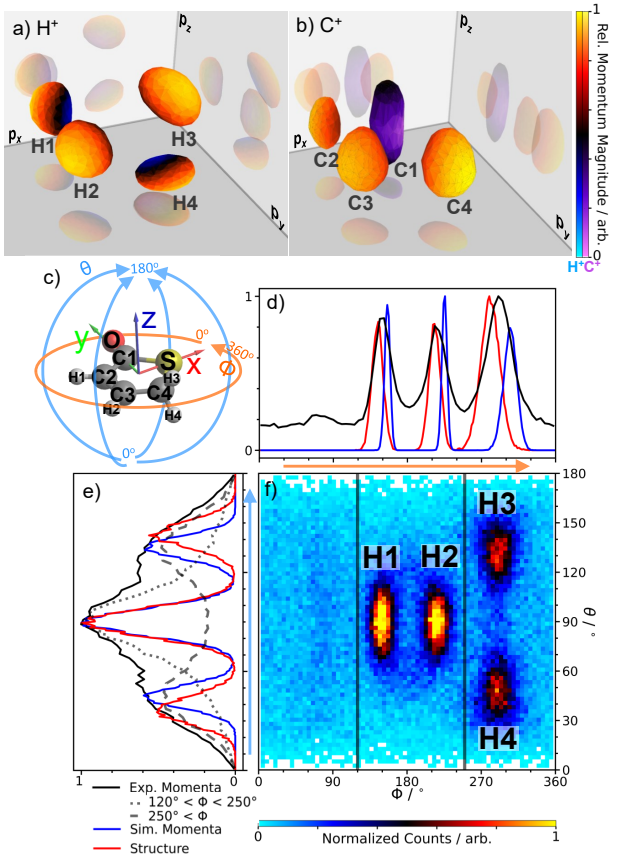


FIG. 3. Different representations of experimental ion momenta. a)-b): 3D isosurfaces of the density of $H^+$ and $C^+$ ion momenta in Cartesian coordinates. The two colorscales represent the (separately normalized) magnitude of the $H^+/C^+$ momenta. c) Definition of spherical polar coordinates $(\phi, \theta)$. f) $H^+$ momenta in spherical polar coordinates. d) and e) projections of f) onto $\phi$ and $\theta$ (black solid lines), and two slices: $120° < \phi < 250°$ (dotted line), $\phi > 250°$ (dashed line). Comparison to Coulomb explosion simulations (blue lines) and bond angles in the real-space structure (red lines) are also given, as described in detail in the main text.

ular structure prior to Coulomb explosion than the other $C^+$ ions.

Since much of the structural information contained within the recorded 3D correlated momentum distributions relate to the angles between different ion momenta, Figures 3d and Fig. 3e compare the observed $H^+$ ejection angles in $\theta$ and $\phi$ to simulations of the Coulomb explosion of cold thiophenone molecules. In both $\theta$ and $\phi$, the peak positions in the experimental data (black lines) agree well with the Coulomb explosion simulations (blue lines), but the experimental angular distributions are broader than those simulated (see Fig. S12 of the SI). Other works have demonstrated that even better overall agreement can often be obtained if the molecular charge-up dynamics are either modeled empirically [20, 68–71] or calculated *ab initio* [5, 72, 73]. Here, however, we stress that such advanced modeling is not required to clearly identify the general structural features of the molecule from the experimental momentum correlations. Agreement between the classical CEI prediction and the experimental data is good even though only four of the ten atomic ions are detected, as was found also in other recent studies of similarly sized molecules [5, 30, 32]. For the present case, we find a very good match between the measured $H^+$ momenta and the interbond angles in the real-space molecular structure (determined and Wigner sampled as described in 'Coulomb Explosion Simulations' section), shown as red lines in Figs. 3d and 3e. For this comparison, the real-space $\theta$ and $\phi$ angles for each C-H bond vector were computed in a coordinate system defined similarly to the Coulomb explosion data: the S and O atoms lie in the $xy$ plane, and the bisector between the two C-S bonds defines the $x$ axis. While such a direct mapping between ion ejection angles and bond angles is not generally the case (see for example the equivalent comparison for the $C^+$ ion in Fig. S11 of the SI, where the peak positions are significantly different), this finding emphasizes that the momenta of the light $H^+$ ions can be very good reporters of the molecular structure as they tend to be ejected along the axis of the C-H bond from which they derive. In the following, we pursue this route further, examining expected changes in the 3D momenta of the $H^+$ ions as the structure of the molecule changes after electronic excitation using UV light.

## DISCUSSION

The photochemistry of thiophenone has attracted significant interest, with recent time-resolved experiments exploring the role of ultrafast ring opening following UV photoexcitation at wavelengths around 267 nm [50–52]. Such excitation populates the optically bright $S_2$ state, of predominant $n\pi^*$ character. The subsequent nonadiabatic relaxation to the $S_1$ and then to the $S_0$ electronic states is driven by nuclear motion along an S-C bond stretch coordinate. Cleavage of this bond initially produces a ring-opened biradical product, from which multiple rapid isomerizations are possible (as shown in the reaction scheme in Fig. S13 of the SI). Using mega-electronvolt ultrafast electron diffraction (UED) and complementary AIMD calculations, time-resolved product branching ratios during this reaction were determined, and a substantial (≈50%) yield of a high-energy episulfide (three-membered ring) isomer was confirmed [52]. However, various ring-opened variants with structures that differ primarily by the relative positions of the H atoms could not be distinguished. Variants of particular interest include the biradical species formed upon photoexcitation (which we henceforth label P0), a thioaldehyde (2-thioxoethylketene, P1) and a thiol (2-(2-sulfanylethyl)ketene, P2), as shown in Fig. 4. Demonstrating that CEI has the potential to resolve these structures is a major goal of the present study.

In line with this goal and in order to explore the

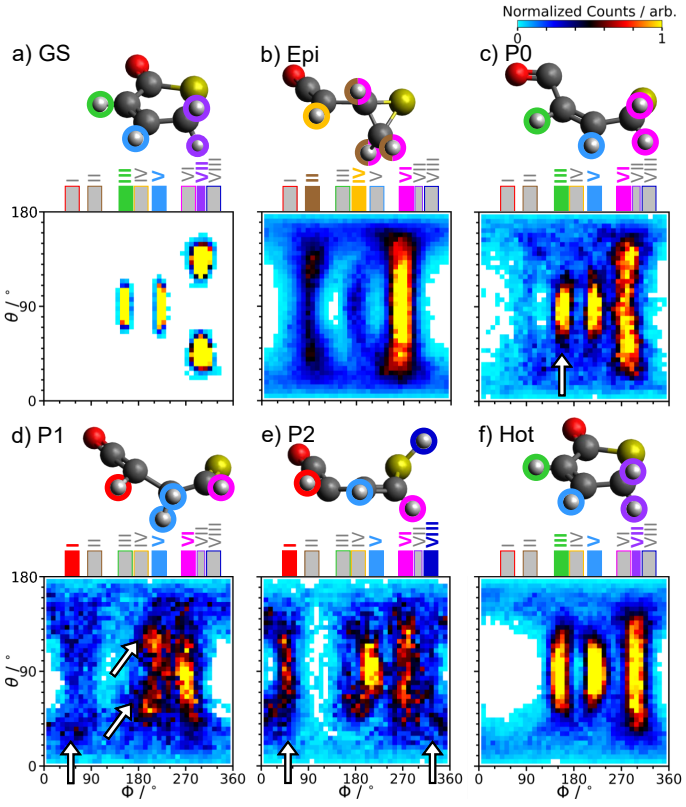


FIG. 4. Simulated three-dimensional $H^+$ momentum distributions (in spherical polar coordinates) predicted for the cold ground state (a), the major episulfide photoproduct (b), and other possible (vibrationally hot) photoproducts of UV-excited thiophenone labeled P0 (c), P1 (d), P2 (e), and hot ground state (f) following prior work [51, 52], as shown by the sketches of the molecular geometry. Specific regions of $\phi$ are labeled (I-VIII) and colored above each panel, with the corresponding H atom color coded to match. The white arrows highlight regions which present unique signatures compared to the other ring-opened products. The colorscale is normalized to the number of coincidences contributing to each panel.

prospects for future time-resolved Coulomb explosion studies of the photoinduced dynamics of thiophenone, we have coupled classical Coulomb explosion simulations with the outputs from previously reported AIMD simulations of the neutral dynamics out to a total time of 2 ps following photoexcitation [51]. By classifying the outputs of the dynamics simulations in terms of different isomeric product species, the final momentum distribution for each of these species can be simulated. The $H^+$ relative momenta associated with these product species are shown in Figs. 4b-f in the spherical-polar coordinate representation. For comparison, results from the previously described simulation of a pool of cold, equilibrium thiophenone structures are shown in Fig. 4a. It closely resembles the experimental signal shown in Fig. 3f despite the simplicity of the Coulomb explosion simulation. The signal for the three-membered episulfide product (Fig. 4b) is predicted at starkly different regions of momentum, highlighting the striking sensitivity of CEI to the 3D molecular structure and the ability to clearly resolve the formation of photoproducts.

In the following, we focus in particular on the molecular-frame $H^+$ momentum distributions for three initially-formed ring-opened species, whose structures differ primarily in the arrangement of hydrogen atoms and which could not be distinguished in previous studies [51, 52]. The $H^+$ relative momenta associated with three ring-opened structures are shown in Figs. 4c through 4e Details on the classification of the different isomers are given in the '*Ab initio* Calculations of Photoinduced Dynamics' section. Simulated signals for the corresponding predicted $C^+$ signals are given in Fig. S14.

In general, the predicted Coulomb explosion signals for the product species are more diffuse than that of the unpumped thiophenone molecule. This is because a large amount of energy has been deposited into vibrational modes following photoexcitation, and the CEI data contain information on the entire vibrational wavepacket. Here we focus on categorizing the structural changes in terms of chemical functionalization (e.g., 'classes' of photoproduct structures). Large differences can be seen (highlighted by the white arrows in Fig. 4) between the expected Coulomb explosion signals for these product families with only minimal changes in functional groups/positions of hydrogens (as shown above each panel). There are clear shifts in the position of features in $\phi$ and changes to the splitting in $\theta$. These large variations in signal should be distinguishable in a time-resolved experiment. A quantitative analysis of the signal in each region is shown in Fig. S15, which demonstrates that certain photoproducts clearly dominate in distinct regions.

In order to help with the assignment of specific features in the momentum distributions to the corresponding hydrogen atoms in the molecule, we have labeled and color coded eight regions of $\phi$ (regions I-VIII) at the top of each panel in Fig. 4 and color coded the hydrogen atoms accordingly. The $H^+$ momentum distribution of the initial ring-opened biradical species (Fig. 4c, P0) shows some similarities with that of the ring-closed parent (Fig. 4a, GS). Bond elongation leads to a small shift of the out-of-plane hydrogens from region VII to VI. A less subtle change is the loss of rigidity accompanying the ring opening allowing some rotation about the C–C bond adjacent to the C–S bond – reflected in the greater spread of the momentum distribution in $\theta$ within region VI. The thioaldehyde (Fig. 4d, P1) and thiol (Fig. 4e, P2) isomers form on a slightly longer time scale [52], each requiring a hydrogen migration from P0. P1 and P2 exhibit signal at $\phi \simeq 50°$ (region I), which is distinct from signals associated with GS and P0 structures. This signal arises from the hydrogen atom adjacent to the ketene (C=C=O) moiety present in these two products. For all the families of structures shown in Fig. 4, the biggest differences in the predicted $H^+$ momenta lies in the signal due to out-of-plane hydrogens. If two hydrogen atoms are bound to a single carbon atom, the signal for both ap-

pears in similar regions of $\phi$ (VII/purple for GS, VI/pink for P0, and V/light blue for P1) but are separated into two regions of intensity in $\theta$, hence there are only three occupied regions of $\phi$. The absence of such out-of-plane hydrogens in P2 leads to signal in an additional region of $\phi$ (near $\phi \simeq 330°$, region VIII) compared to P0 and P1, i.e., one for each of the four hydrogens.

It should be noted that the molecular frame in which these data have been analyzed was chosen for intuitive interpretation in the case of thiophenone at equilibrium and then kept consistent for all products. Given the rich and multidimensional nature of the correlated ion momenta, alternative molecular frames can be devised for specific products to extract clearer or more intuitive structural information. Developing robust methods to identify the optimum molecular frame for a given molecular structure or family of structures is an ongoing challenge. Possible directions are the use of principal component analysis [74] or other machine learning approaches [75] that can take advantage of the highly multidimensional correlations intrinsic to the CEI data to separate different molecular geometries.

In summary, we have shown how X-ray-induced Coulomb explosion imaging of an organic molecule can provide well-resolved structural information through detection of the 3D momentum vectors of the $H^+$ fragment ions stemming from the peripheral hydrogen atoms on the molecule. Employing the information extracted from these messenger ions, together with Coulomb explosion simulations of photo-induced molecular dynamics predicted by quantum calculations, offers a route to direct observation of the neutral fragmentation dynamics of isolated molecules at the level of individual atoms and with femtosecond time resolution – especially when combined with emerging high-repetition rate optical and X-ray laser sources and more advanced multi-dimensional data analysis techniques [75]. This will allow extension of the approach well beyond thiophenone (the molecular target in the demonstrations reported here), to enable generalized imaging of ultrafast photoinduced motion in isolated organic molecules.

## METHODS

### Experiment

The experiment was performed using the Cold Target Recoil Ion Momentum Spectroscopy (COLTRIMS) reaction microscope (REMI) [76, 77] end-station of the Small Quantum Systems (SQS) scientific instrument at the European XFEL [59]. This instrument has been described in previous publications [5, 20, 78–80], and the experiment is depicted schematically in Fig. 1.

Vapor of 2(5H)-thiophenone ($C_4H_4OS$) was generated by heating an out-of-vacuum reservoir to 50-60 °C. A supersonic gas jet was formed using 200 mbar of helium as carrier gas, expanding the mixture into vacuum through a nozzle of 200 $\mu$m diameter, and collimating it by three skimmers and a set of adjustable slits. Gas line, nozzle, and the first section of the jet vacuum chamber were also heated to 60 °C to prevent condensation. The base pressure in the interaction chamber was maintained at $1 \times 10^{-11}$ mbar during operation. Achieving such low background pressure is key in the ability of the current work to identify coincidences involving $H^+$ ions with little contamination from false coincidences originating from ionization of background molecules. The molecular beam was crossed with the X-ray beam at 90° in the center of the reaction microscope. At the interaction point, a high extraction field of $E = 400$ V/cm was applied for the first 6 cm of the ion flight direction, followed by a 12 cm long field-free drift region. Fragment ions created by the X-ray ionization were extracted towards a time- and position-sensitive large-area microchannel-plate detector (120 mm diameter) with hexagonal delay-line position readout. The recorded ion mass spectrum is shown in Fig. S6. The ions originating from each X-ray pulse were measured in coincidence. The analog detector signals were recorded at 10 Hz with fast analog-to-digital converters. An average of 1.6 ion hits/pulse were recorded, of which 0.5 ion hits/pulse came from residual gas not originating from the molecular beam. For the data presented in Figures 1-3, 133,966 relevant Coulomb explosion events (defined as the coincident detection of one $O^+$, one $S^+$, and at least one $H^+$ and one $C^+$ ion) were collected over 26,003,258 FEL shots ($\sim$ 8.5 hours of data acquisition).

The FEL operated at a base repetition rate of 10 Hz, providing bursts of electron pulses with an internal spacing of 1.1 MHz. Out of these, we used 84 bunches to generate X-ray pulses with an intra-pulse spacing of 188 kHz, resulting in an effective repetition rate of the experiment of 840 Hz. The photon energy was 2.6 keV, which is above the sulfur 1$s$ ionization edge. The single-shot X-ray pulse energy was measured upstream of the beamline mirrors by a gas monitor detector; it was 1.4-1.8 mJ throughout the beamtime. The total beamline transmission was estimated to be 85% at 2.6 keV for the beamline configuration during this user run (run 8) [81], resulting in 1.2-1.5 mJ on target. The X-ray pulses were focused by a pair of bendable Kirkpatrick-Baez mirrors to a focus point 4.7 m downstream of the second (horizontal) focusing mirror. In a separate measurement campaign at a similar focal distance (ca. 4.1 m), the focus size was characterized by imprint measurements to be $< 5\,\mu m$ (FWHM). The pulse duration of the X-ray pulses is not measured directly, but can be estimated from statistical analysis of single-shot X-ray spectra recorded in the fifth diffraction order of the grating spectrometer in the SASE3 tunnel during machine tuning before the beamtime. The measured quasi-monochromatic group duration of 3 fs and the measured bandwidth of 0.4% result in an estimated total X-ray pulse duration of 6 fs when assuming a linear chirp of the pulse [82].

### Data Processing

The data processing and analysis procedure followed is similar to that described previously [5, 32]. The recorded $x$, $y$ position of each ion gives its momentum along the $x$ and $y$ axes. The ion flight times can be converted to the momentum along the $z$ dimension of the spectrometer. The absolute momentum scale was calibrated by recording data for the X-ray ionization of $N_2$ and comparing the kinetic energy release (KER) distributions for fragmentation into $N^+ + N^+$ to literature values [83, 84].

The laboratory-frame momentum distributions are then transformed to a molecular frame where all molecules have the same orientation using coincidence analysis by considering laser shots in which we detect at least one $S^+$, $O^+$, $C^+$, and $H^+$ ion (4-fold coincidence). On a shot-by-shot basis, the momenta of these sets of ions are aligned onto a common orientation for all shots, a 'molecular' frame, in which all other detected ions of the same species are plotted.

Particularly for larger, more complex molecules, there are many different ways in which this molecular frame can be constructed. In the case of thiophenone, one intuitive frame, adopted in Fig. 2, can be formed by fixing the momentum of the sulfur atom along a given vector ($+x$), and defining a plane by this S vector and that of the oxygen momentum (the $xy$ plane) for every shot. The frame is chosen such that the $y$ component of the oxygen ion momentum is positive. Other ions are rotated relative to this, as shown schematically in Fig. S1. For the sake of this paper, this rotation is completed for four ions ($S^+$, $O^+$, $C^+$ and $H^+$) at a time. In cases where more than one of each ion species are detected in a single shot, the rotation is completed for all possible combinations of sets of four ions. Two-dimensional projections of the resultant 3D relative ion momentum distributions for each ion species are given in Figs. S2 and S3 on a normalized and absolute momentum scale, respectively.

In all representations of the data given, a weak and diffuse feature is spread over all angles resulting mainly from false coincidences - arising from the possibility of Coulomb exploding more than one molecule in a given laser shot. To limit this, momentum filters ($180 < O^+ < 290$, $180 < S^+ < 320$, in atomic units of momenta) have been applied on the $O^+$ and $S^+$ ions in order to reject some of the false coincidences, improving the resultant coincident $H^+$ and $C^+$ ion momentum distributions.

These coincident datasets are inherently high-dimensional, therefore there are many ways of representing the data, some of which are displayed in the main text and are expanded upon in the SI. Figure S4 shows two-dimensional projections of the three-dimensional coincident momentum distributions of $H^+$, $C^+$, $S^+$ and $O^+$ ions in a frame where the $O^+$ momentum is instead used to define the reference ($+x$) vector, while Fig. S5 shows a different data representation as a 3D scatter plot.

### Coulomb Explosion Simulations

To help interpret the experimental data, and to predict the Coulomb explosion signatures of possible structures of photoexcited thiophenone, classical Coulomb explosion simulations were performed [20, 32, 58]. In these simulations, the atom at each site in a given molecular structure is replaced by the corresponding singly charged atomic ion. Using Coulomb's law, the forces on each ion are determined, and the resulting set of Newton's equations of motion are numerically integrated. The final velocities of each ion are then converted to a momentum, and these momenta are analysed and converted to a molecular frame in an analogous way to the experimental data. For the simulations of the Coulomb explosion of thiophenone at equilibrium, we sampled 10,000 geometries from a Wigner distribution at a temperature of 60 K, and simulated the Coulomb explosion of each geometry in this pool [58]. The equilibrium structure and its normal modes were obtained using DFT-B3LYP/aug-cc-pVDZ in the Gaussian 09 [85] software package. The Wigner sampling was done using the Newton-X software [86], where the finite temperature is included as a broadening by a factor $tanh(\hbar\omega/2k_BT)$. A direct comparison of the simulations to the experimental data is given in Figs. S7-S9.

To simulate the explosion patterns of the photoproduct species, the input molecular geometries and velocities of each atom in the neutral species at each time step were obtained from previously published dynamics simulations of photoexcited thiophenone [51, 52], as summarized below.

### *Ab initio* Calculations of Photoinduced Dynamics

The *ab initio* molecular dynamics simulations of the photoinduced dynamics of thiophenone have been described previously [51, 52]. Briefly, nonadiabatic dynamics were simulated using Tully's fewest-switches trajectory surface hopping [87], describing the electronic structure at the SA(4)-CASSCF(10/8)/6-31G* level of theory. The trajectory calculation used the SHARC package [88], whilst Molpro 2012 was used for the electronic structure [89, 90]. Initial structures were sampled from a Wigner distribution and initialized on the $S_2$ state. Upon reaching the ground electronic state, each trajectory was propagated until leaving the region of strong nonadiabaticity between $S_1$ and $S_0$. After this, ground-state *ab initio* Born-Oppenheimer molecular dynamics (BOMD) trajectories were simulated, using the final step of the nonadiabatic molecular dynamics trajectory to provide initial conditions. The ground-state electronic structure was calculated using unrestricted DFT employing the PBE0 exchange/correlation functional and the 6-31G* basis set, using the TeraChem software package [91, 92].

The outputs of the trajectory simulations were then categorized by photoproduct species, for delays between

1 and 2 ps. The decision tree used for this classification has been described in previous publications [51, 52] (e.g., see Fig. S4 in the Supporting Information of Ref. 52). Following classification, the Coulomb explosion of each structure was then simulated as described in the previous section. Figure 4 shows the simulated molecular-frame $H^+$ signals, whereas similar data for $C^+$ are shown in Fig. S14.

## ACKNOWLEDGMENTS

We acknowledge the European XFEL in Schenefeld, Germany, for the provision of x-ray free-electron laser beamtime at the SQS instrument and thank the EuXFEL staff for their assistance. AEG was supported by the European Union, through Horizon Europe project 123-CO: 101067645. Views and opinions expressed are however those of the authors only and do not necessarily reflect those of the European Union. Neither the European Union nor the granting authority can be held responsible for them. HVSL, EW, AR, and DR were supported by the Chemical Sciences, Geosciences, and Biosciences Division, Office of Basic Energy Sciences, Office of Science, US Department of Energy, grant no. DE-FG02-86ER13491. KC and SB were supported by grant no. DE-SC0020276 and PMW by grant no. DE-SC0017995 from the same funding agency. ASV was supported by the National Science Foundation grant no. PHYS-2409365. BFEC acknowledges funding from the European Research Council (ERC) under the European Union's Horizon 2020 research and innovation programme (Grant agreement No. 803718, project SINDAM) and from EPSRC for the grants EP/V026690/1, EP/Y01930X/1, and EP/X026973/1. MBr and JWM gratefully acknowledge support provided by the UK Engineering and Physical Sciences Research Council for funding through Programme Grant EP/V026690/1. MBu and EMW are grateful to the EPSRC for support from EP/S028617/1. FT acknowledges funding by the Deutsche Forschungsgemeinschaft (DFG, German Research Foundation) - Project 509471550, Emmy Noether Programme. HS acknowledges support from Villum Fonden through Villum Investigator Grant No. 25886. LMI acknowledges funding by a public grant from the Laboratoire d'Excellence Physics Atoms Light Matter (LabEx PALM) overseen by the French National Research Agency (ANR) as part of the "Investissements d'Avenir" program (reference: ANR-10-LABX-0039-PALM), by the ANR Q-DeLight project, Grant No. ANR-20-CE29-0014 of the French Agence Nationale de la Recherche.

**Data availability**

Data recorded for the experiment at the European XFEL are available at [93].

**Associated Content**

Supporting information is available containing additional data representations and simulations.

[1] M. G. Pullen, B. Wolter, A.-T. Le, M. Baudisch, M. Hemmer, A. Senftleben, C. D. Schröter, J. Ullrich, R. Moshammer, C.-D. Lin, et al., Imaging an aligned polyatomic molecule with laser-induced electron diffraction, Nature Communications **6**, 7262 (2015).

[2] M. Centurion, T. J. Wolf, and J. Yang, Ultrafast imaging of molecules with electron diffraction, Annual Review of Physical Chemistry **73**, 21 (2022).

[3] B. Stankus, H. Yong, J. Ruddock, L. Ma, A. M. Carrascosa, N. Goff, S. Boutet, X. Xu, N. Zotev, A. Kirrander, et al., Advances in ultrafast gas-phase X-ray scattering, Journal of Physics B: Atomic, Molecular and Optical Physics **53**, 234004 (2020).

[4] A. Odate, A. Kirrander, P. M. Weber, and M. P. Minitti, Brighter, faster, stronger: ultrafast scattering of free molecules, Advances in Physics: X **8**, 2126796 (2023).

[5] R. Boll, J. M. Schäfer, B. Richard, K. Fehre, G. Kastirke, Z. Jurek, M. S. Schöffler, M. M. Abdullah, N. Anders, T. M. Baumann, et al., X-ray multiphoton-induced Coulomb explosion images complex single molecules, Nature Physics **18**, 423 (2022).

[6] C. S. Slater, S. Blake, M. Brouard, A. Lauer, C. Vallance, J. J. John, R. Turchetta, A. Nomerotski, L. Christensen, J. H. Nielsen, et al., Covariance imaging experiments using a pixel-imaging mass-spectrometry camera, Physical Review A **89**, 011401 (2014).

[7] B. Ulrich, A. Vredenborg, A. Malakzadeh, L. P. H. Schmidt, T. Havermeier, M. Meckel, K. Cole, M. Smolarski, Z. Chang, T. Jahnke, et al., Imaging of the structure of the argon and neon dimer, trimer, and tetramer, The Journal of Physical Chemistry A **115**, 6936 (2011).

[8] J. Voigtsberger, S. Zeller, J. Becht, N. Neumann, F. Sturm, H.-K. Kim, M. Waitz, F. Trinter, M. Kunitski, A. Kalinin, et al., Imaging the structure of the trimer systems $^4He_3$ and $^3He^4He_2$, Nature Communications **5**, 5765 (2014).

[9] M. Kunitski, S. Zeller, J. Voigtsberger, A. Kalinin, L. P. H. Schmidt, M. Schöffler, A. Czasch, W. Schöllkopf, R. E. Grisenti, T. Jahnke, et al., Observation of the Efimov state of the helium trimer, Science **348**, 551 (2015).

[10] L. Holmegaard, J. H. Nielsen, I. Nevo, H. Stapelfeldt, F. Filsinger, J. Küpper, and G. Meijer, Laser-induced alignment and orientation of quantum-state-selected large molecules, Physical Review Letters **102**, 023001 (2009).

[11] J. J. Larsen, K. Hald, N. Bjerre, H. Stapelfeldt, and T. Seideman, Three dimensional alignment of molecules using elliptically polarized laser fields, Physical Review Letters **85**, 2470 (2000).

[12] K. F. Lee, D. Villeneuve, P. Corkum, A. Stolow, and J. G. Underwood, Field-free three-dimensional alignment of polyatomic molecules, Physical Review Letters **97**, 173001 (2006).

[13] J. D. Pickering, B. Shepperson, B. A. Hübschmann, F. Thorning, and H. Stapelfeldt, Alignment and imaging of the $CS_2$ dimer inside helium nanodroplets, Physical

Review Letters **120**, 113202 (2018).
[14] C. A. Schouder, A. S. Chatterley, J. D. Pickering, and H. Stapelfeldt, Laser-induced Coulomb explosion imaging of aligned molecules and molecular dimers, Annual Review of Physical Chemistry **73**, 323 (2022).
[15] J. Gagnon, K. F. Lee, D. Rayner, P. Corkum, and V. Bhardwaj, Coincidence imaging of polyatomic molecules via laser-induced Coulomb explosion, Journal of Physics B: Atomic, Molecular and Optical Physics **41**, 215104 (2008).
[16] M. Pitzer, M. Kunitski, A. S. Johnson, T. Jahnke, H. Sann, F. Sturm, L. P. H. Schmidt, H. Schmidt-Böcking, R. Dörner, J. Stohner, et al., Direct determination of absolute molecular stereochemistry in gas phase by Coulomb explosion imaging, Science **341**, 1096 (2013).
[17] U. Ablikim, C. Bomme, H. Xiong, E. Savelyev, R. Obaid, B. Kaderiya, S. Augustin, K. Schnorr, I. Dumitriu, T. Osipov, et al., Identification of absolute geometries of cis and trans molecular isomers by Coulomb explosion imaging, Scientific Reports **6**, 38202 (2016).
[18] K. Nagaya, K. Motomura, E. Kukk, H. Fukuzawa, S. Wada, T. Tachibana, Y. Ito, S. Mondal, T. Sakai, K. Matsunami, et al., Ultrafast dynamics of a nucleobase analogue illuminated by a short intense X-ray free electron laser pulse, Physical Review X **6**, 021035 (2016).
[19] M. Burt, K. Amini, J. W. Lee, L. Christiansen, R. R. Johansen, Y. Kobayashi, J. D. Pickering, C. Vallance, M. Brouard, and H. Stapelfeldt, Communication: Gas-phase structural isomer identification by Coulomb explosion of aligned molecules, The Journal of Chemical Physics **148**, 091102 (2018).
[20] X. Li, A. Rudenko, M. Schöffler, N. Anders, T. M. Baumann, S. Eckart, B. Erk, A. De Fanis, K. Fehre, R. Dörner, et al., Coulomb explosion imaging of small polyatomic molecules with ultrashort X-ray pulses, Physical Review Research **4**, 013029 (2022).
[21] T. Jahnke, S. Mai, S. Bhattacharyya, K. Chen, R. Boll, et al., Direct observation of ultrafast symmetry reduction during internal conversion of 2-thiouracil using coulomb explosion imaging, Nature Communications **16**, 2074 (2025).
[22] J. L. Hansen, J. H. Nielsen, C. B. Madsen, A. T. Lindhardt, M. P. Johansson, T. Skrydstrup, L. B. Madsen, and H. Stapelfeldt, Control and femtosecond time-resolved imaging of torsion in a chiral molecule, The Journal of Chemical Physics **136**, 204310 (2012).
[23] L. Christensen, J. H. Nielsen, C. B. Brandt, C. B. Madsen, L. B. Madsen, C. S. Slater, A. Lauer, M. Brouard, M. P. Johansson, B. Shepperson, et al., Dynamic Stark control of torsional motion by a pair of laser pulses, Physical Review Letters **113**, 073005 (2014).
[24] X. Li, R. Boll, P. Vindel-Zandbergen, J. González-Vázquez, D. E. Rivas, S. Bhattacharyya, K. Borne, K. Chen, A. De Fanis, B. Erk, et al., Imaging a light-induced molecular elimination reaction with an X-ray free-electron laser, Nature Communications **16**, 7006 (2025).
[25] S. Pathak, R. Obaid, S. Bhattacharyya, J. Bürger, X. Li, J. Tross, T. Severt, B. Davis, R. C. Bilodeau, C. A. Trallero-Herrero, et al., Differentiating and quantifying gas-phase conformational isomers using Coulomb explosion imaging, The Journal of Physical Chemistry Letters **11**, 10205 (2020).
[26] E. G. Champenois, N. H. List, M. Ware, M. Britton, P. H. Bucksbaum, X. Cheng, M. Centurion, J. P. Cryan, R. Forbes, I. Gabalski, et al., Femtosecond electronic and hydrogen structural dynamics in ammonia imaged with ultrafast electron diffraction, Physical Review Letters **131**, 143001 (2023).
[27] I. Gabalski, A. Green, P. Lenzen, F. Allum, M. Bain, S. Bhattacharyya, M. A. Britton, E. G. Champenois, X. Cheng, J. P. Cryan, et al., Imaging valence electron rearrangement in a chemical reaction using hard x-ray scattering, arXiv preprint arXiv:2506.19172 (2025).
[28] T. Wang, H. Jiang, M. Zhang, X. Zou, P. Zhu, F. He, Z. Li, and D. Xiang, Probing valence electron and hydrogen dynamics using charge-pair imaging with ultrafast electron diffraction, arXiv preprint arXiv:2506.21047 (2025).
[29] Z. Vager, R. Naaman, and E. Kanter, Coulomb explosion imaging of small molecules, Science **244**, 426 (1989).
[30] H. Yuan, Y. Gao, B. Yang, S. Gu, H. Lin, D. Guo, J. Liu, S. Zhang, X. Ma, and S. Xu, Coulomb explosion imaging of complex molecules using highly charged ions, Physical Review Letters **133**, 193002 (2024).
[31] F. Légaré, K. F. Lee, I. Litvinyuk, P. Dooley, S. Wesolowski, P. Bunker, P. Dombi, F. Krausz, A. Bandrauk, D. M. Villeneuve, et al., Laser Coulomb-explosion imaging of small molecules, Physical Review A **71**, 013415 (2005).
[32] H. V. S. Lam, A. S. Venkatachalam, S. Bhattacharyya, K. Chen, K. Borne, E. Wang, R. Boll, T. Jahnke, V. Kumarappan, A. Rudenko, et al., Differentiating three-dimensional molecular structures using laser-induced Coulomb explosion imaging, Physical Review Letters **132**, 123201 (2024).
[33] H. Stapelfeldt, E. Constant, and P. Corkum, Wave packet structure and dynamics measured by Coulomb explosion, Physical Review Letters **74**, 3780 (1995).
[34] H. Stapelfeldt, E. Constant, H. Sakai, and P. B. Corkum, Time-resolved Coulomb explosion imaging: A method to measure structure and dynamics of molecular nuclear wave packets, Physical Review A **58**, 426 (1998).
[35] P. W. Dooley, I. V. Litvinyuk, K. F. Lee, D. M. Rayner, M. Spanner, D. M. Villeneuve, and P. B. Corkum, Direct imaging of rotational wave-packet dynamics of diatomic molecules, Physical Review A **68**, 023406 (2003).
[36] I. Bocharova, A. Alnaser, U. Thumm, T. Niederhausen, D. Ray, C. L. Cocke, and I. Litvinyuk, Time-resolved Coulomb-explosion imaging of nuclear wave-packet dynamics induced in diatomic molecules by intense few-cycle laser pulses, Physical Review A **83**, 013417 (2011).
[37] T. Ergler, A. Rudenko, B. Feuerstein, K. Zrost, C. Schröter, R. Moshammer, and J. Ullrich, Spatiotemporal imaging of ultrafast molecular motion: Collapse and revival of the $D_2^+$ nuclear wave packet, Physical Review Letters **97**, 193001 (2006).
[38] M. Burt, R. Boll, J. W. Lee, K. Amini, H. Köckert, C. Vallance, A. S. Gentleman, S. R. Mackenzie, S. Bari, C. Bomme, et al., Coulomb-explosion imaging of concurrent $CH_2BrI$ photodissociation dynamics, Physical Review A **96**, 043415 (2017).
[39] F. Allum, M. Burt, K. Amini, R. Boll, H. Köckert, P. K. Olshin, S. Bari, C. Bomme, F. Braße, B. Cunha de Miranda, et al., Coulomb explosion imaging of $CH_3I$ and $CH_2ClI$ photodissociation dynamics, The Journal of Chemical Physics **149**, 204313 (2018).
[40] M. Corrales, J. González-Vázquez, R. De Nalda, and

L. Bañares, Coulomb explosion imaging for the visualization of a conical intersection, The Journal of Physical Chemistry Letters **10**, 138 (2018).

[41] T. Endo, S. P. Neville, V. Wanie, S. Beaulieu, C. Qu, J. Deschamps, P. Lassonde, B. E. Schmidt, H. Fujise, M. Fushitani, et al., Capturing roaming molecular fragments in real time, Science **370**, 1072 (2020).

[42] H. Ibrahim, B. Wales, S. Beaulieu, B. E. Schmidt, N. Thiré, E. P. Fowe, É. Bisson, C. T. Hebeisen, V. Wanie, M. Giguére, et al., Tabletop imaging of structural evolutions in chemical reactions demonstrated for the acetylene cation, Nature Communications **5**, 4422 (2014).

[43] E. Wang, S. Bhattacharyya, K. Chen, K. Borne, F. Ziaee, S. Pathak, H. V. S. Lam, A. S. Venkatachalam, X. Chen, R. Boll, et al., Time-resolved Coulomb explosion imaging unveils ultrafast ring opening of furan, arXiv preprint arXiv:2311.05099 (2023).

[44] B. Erk, D. Rolles, L. Foucar, B. Rudek, S. W. Epp, M. Cryle, C. Bostedt, S. Schorb, J. Bozek, A. Rouzee, et al., Inner-shell multiple ionization of polyatomic molecules with an intense X-ray free-electron laser studied by coincident ion momentum imaging, Journal of Physics B: Atomic, Molecular and Optical Physics **46**, 164031 (2013).

[45] B. Erk, D. Rolles, L. Foucar, B. Rudek, S. W. Epp, M. Cryle, C. Bostedt, S. Schorb, J. Bozek, A. Rouzee, et al., Ultrafast charge rearrangement and nuclear dynamics upon inner-shell multiple ionization of small polyatomic molecules, Physical Review Letters **110**, 053003 (2013).

[46] K. Motomura, E. Kukk, H. Fukuzawa, S.-i. Wada, K. Nagaya, S. Ohmura, S. Mondal, T. Tachibana, Y. Ito, R. Koga, et al., Charge and nuclear dynamics induced by deep inner-shell multiphoton ionization of $CH_3I$ molecules by intense X-ray free-electron laser pulses, The Journal of Physical Chemistry Letters **6**, 2944 (2015).

[47] T. Takanashi, K. Nakamura, E. Kukk, K. Motomura, H. Fukuzawa, K. Nagaya, S.-i. Wada, Y. Kumagai, D. Iablonskyi, Y. Ito, et al., Ultrafast Coulomb explosion of a diiodomethane molecule induced by an X-ray free-electron laser pulse, Physical Chemistry Chemical Physics **19**, 19707 (2017).

[48] E. Kukk, K. Motomura, H. Fukuzawa, K. Nagaya, and K. Ueda, Molecular dynamics of XFEL-induced photodissociation, revealed by ion-ion coincidence measurements, Applied Sciences **7**, 531 (2017).

[49] E. Kukk, H. Myllynen, K. Nagaya, S. Wada, J. D. Bozek, T. Takanashi, D. You, A. Niozu, K. Kooser, T. Gaumnitz, et al., Coulomb implosion of tetrabromothiophene observed under multiphoton ionization by free-electron-laser soft-X-ray pulses, Physical Review A **99**, 023411 (2019).

[50] D. Murdock, S. J. Harris, J. Luke, M. P. Grubb, A. J. Orr-Ewing, and M. N. Ashfold, Transient UV pump–IR probe investigation of heterocyclic ring-opening dynamics in the solution phase: The role played by $n\sigma^*$ states in the photoinduced reactions of thiophenone and furanone, Physical Chemistry Chemical Physics **16**, 21271 (2014).

[51] S. Pathak, L. M. Ibele, R. Boll, C. Callegari, A. Demidovich, B. Erk, R. Feifel, R. Forbes, M. Di Fraia, L. Giannessi, et al., Tracking the ultraviolet-induced photochemistry of thiophenone during and after ultrafast ring opening, Nature Chemistry **12**, 795 (2020).

[52] J. P. F. Nunes, L. M. Ibele, S. Pathak, A. R. Attar, S. Bhattacharyya, R. Boll, K. Borne, M. Centurion, B. Erk, M.-F. Lin, et al., Monitoring the evolution of relative product populations at early times during a photochemical reaction, Journal of the American Chemical Society **146**, 4134 (2024).

[53] A. Hishikawa, A. Matsuda, M. Fushitani, and E. J. Takahashi, Visualizing recurrently migrating hydrogen in acetylene dication by intense ultrashort laser pulses, Physical Review Letters **99**, 258302 (2007).

[54] A. Hishikawa, A. Matsuda, E. J. Takahashi, and M. Fushitani, Acetylene-vinylidene isomerization in ultrashort intense laser fields studied by triple ion-coincidence momentum imaging, The Journal of Chemical Physics **128** (2008).

[55] A. Matsuda, M. Fushitani, E. J. Takahashi, and A. Hishikawa, Visualizing hydrogen atoms migrating in acetylene dication by time-resolved three-body and four-body Coulomb explosion imaging, Physical Chemistry Chemical Physics **13**, 8697 (2011).

[56] C. E. Liekhus-Schmaltz, I. Tenney, T. Osipov, A. Sanchez-Gonzalez, N. Berrah, R. Boll, C. Bomme, C. Bostedt, J. D. Bozek, S. Carron, et al., Ultrafast isomerization initiated by X-ray core ionization, Nature Communications **6**, 8199 (2015).

[57] C.-M. Tseng, M. Fushitani, A. Matsuda, and A. Hishikawa, Coincidence momentum imaging of four-and three-body Coulomb explosion of formaldehyde in ultrashort intense laser fields, Journal of Electron Spectroscopy and Related Phenomena **228**, 25 (2018).

[58] S. Bhattacharyya, K. Borne, F. Ziaee, S. Pathak, E. Wang, A. S. Venkatachalam, X. Li, N. Marshall, K. D. Carnes, C. W. Fehrenbach, et al., Strong-field-induced Coulomb explosion imaging of tribromomethane, The Journal of Physical Chemistry Letters **13**, 5845 (2022).

[59] W. Decking, S. Abeghyan, P. Abramian, A. Abramsky, A. Aguirre, C. Albrecht, P. Alou, M. Altarelli, P. Altmann, K. Amyan, et al., A MHz-repetition-rate hard X-ray free-electron laser driven by a superconducting linear accelerator, Nature Photonics **14**, 391 (2020).

[60] L. Frasinski, K. Codling, and P. Hatherly, Covariance mapping: A correlation method applied to multiphoton multiple ionization, Science **246**, 1029 (1989).

[61] F. Allum, C. Cheng, A. J. Howard, P. H. Bucksbaum, M. Brouard, T. Weinacht, and R. Forbes, Multi-particle three-dimensional covariance imaging:"coincidence" insights into the many-body fragmentation of strong-field ionized $D_2O$, The Journal of Physical Chemistry Letters **12**, 8302 (2021).

[62] L. J. Frasinski, Cumulant mapping as the basis of multi-dimensional spectrometry, Physical Chemistry Chemical Physics **24**, 20776 (2022).

[63] C. Cheng, L. J. Frasinski, G. Moğol, F. Allum, A. J. Howard, D. Rolles, P. H. Bucksbaum, M. Brouard, R. Forbes, and T. Weinacht, Multiparticle cumulant mapping for Coulomb explosion imaging, Physical Review Letters **130**, 093001 (2023).

[64] C. Cheng, L. J. Frasinski, G. Moğol, F. Allum, A. J. Howard, P. H. Bucksbaum, R. Forbes, and T. Weinacht, Multiparticle cumulant mapping for Coulomb explosion imaging: Calculations and algorithm, Physical Review A **109**, 042802 (2024).

[65] J. W. McManus, F. Allum, J. Featherstone, C.-S. Lam,

and M. Brouard, Two-dimensional projected-momentum covariance mapping for Coulomb explosion imaging, The Journal of Physical Chemistry A **128**, 3220 (2024).

[66] A. Sayler, E. Eckner, J. McKenna, B. Esry, K. Carnes, I. Ben-Itzhak, and G. Paulus, Nonunique and nonuniform mapping in few-body Coulomb-explosion imaging, Physical Review A **97**, 033412 (2018).

[67] L. Kranabetter, H. H. Kristensen, C. A. Schouder, and H. Stapelfeldt, Structure determination of alkali trimers on helium nanodroplets through laser-induced Coulomb explosion, The Journal of Chemical Physics **160**, 131101 (2024).

[68] N. Saito, Y. Muramatsu, H. Chiba, K. Ueda, K. Kubozuka, I. Koyano, K. Okada, O. Jagutzki, A. Czasch, T. Weber, M. Hattass, H. Schmidt-Böcking, R. Moshammer, M. Lavollée, and U. Becker, Deformation, nuclear motion and fragmentation of core-excited $CO_2$ probed by multiple-ion coincidence momentum imaging, Journal of Electron Spectroscopy and Related Phenomena **141**, 183 (2004).

[69] K. Nagaya, K. Motomura, E. Kukk, Y. Takahashi, K. Yamazaki, S. Ohmura, H. Fukuzawa, S. Wada, S. Mondal, T. Tachibana, et al., Femtosecond charge and molecular dynamics of I-containing organic molecules induced by intense X-ray free-electron laser pulses, Faraday Discussions **194**, 537 (2016).

[70] H. Fukuzawa and K. Ueda, X-ray induced ultrafast dynamics in atoms, molecules, and clusters: experimental studies at an X-ray free-electron laser facility SACLA and modelling, Advances in Physics: X **5**, 1785327 (2020).

[71] X. Li, R. Boll, D. Rolles, and A. Rudenko, Simple model for sequential multiphoton ionization by ultraintense X-rays, Physical Review A **104**, 033115 (2021).

[72] Z. Jurek, S.-K. Son, B. Ziaja, and R. Santra, XMDYN and XATOM: versatile simulation tools for quantitative modeling of X-ray free-electron laser induced dynamics of matter, Journal of Applied Crystallography **49**, 1048 (2016).

[73] P. J. Ho, D. Ray, C. S. Lehmann, A. E. Fouda, R. W. Dunford, E. P. Kanter, G. Doumy, L. Young, D. A. Walko, X. Zheng, et al., X-ray induced electron and ion fragmentation dynamics in IBr, The Journal of Chemical Physics **158**, 134304 (2023).

[74] B. Richard, J. M. Schäfer, Z. Jurek, R. Santra, and L. Inhester, Statistical analysis of correlations in the X-ray induced Coulomb explosion of iodopyridine, Journal of Physics B: Atomic, Molecular and Optical Physics **54**, 194001 (2021).

[75] A. S. Venkatachalam, L. Greenman, J. Stallbaumer, A. Rudenko, D. Rolles, and H. V. S. Lam, Exploiting correlations in multi-coincidence coulomb explosion patterns for differentiating molecular structures using machine learning, submitted to Nature Communications (2025).

[76] R. Dörner, V. Mergel, O. Jagutzki, L. Spielberger, J. Ullrich, R. Moshammer, and H. Schmidt-Böcking, Cold target recoil ion momentum spectroscopy: a 'momentum microscope' to view atomic collision dynamics, Physics Reports **330**, 95 (2000).

[77] J. Ullrich, R. Moshammer, A. Dorn, R. Dörner, L. P. H. Schmidt, and H. Schmidt-Böcking, Recoil-ion and electron momentum spectroscopy: reaction-microscopes, Reports on Progress in Physics **66**, 1463 (2003).

[78] G. Kastirke, M. S. Schöffler, M. Weller, J. Rist, R. Boll, N. Anders, T. M. Baumann, S. Eckart, B. Erk, A. De Fanis, et al., Photoelectron diffraction imaging of a molecular breakup using an X-ray free-electron laser, Physical Review X **10**, 021052 (2020).

[79] G. Kastirke, M. S. Schöffler, M. Weller, J. Rist, R. Boll, N. Anders, T. M. Baumann, S. Eckart, B. Erk, A. De Fanis, et al., Double core-hole generation in $O_2$ molecules using an X-ray free-electron laser: Molecular-frame photoelectron angular distributions, Physical Review Letters **125**, 163201 (2020).

[80] T. Jahnke, R. Guillemin, L. Inhester, S.-K. Son, G. Kastirke, M. Ilchen, J. Rist, D. Trabert, N. Melzer, N. Anders, et al., Inner-shell-ionization-induced femtosecond structural dynamics of water molecules imaged at an X-ray free-electron laser, Physical Review X **11**, 041044 (2021).

[81] T. M. Baumann, R. Boll, A. De Fanis, P. Grychtol, M. Ilchen, U. F. Jastrow, M. Kato, C. Lechner, T. Maltezopoulos, T. Mazza, et al., Harmonic radiation contribution and X-ray transmission at the Small Quantum Systems instrument of European XFEL, Journal of Synchrotron Radiation **30**, 662–670 (2023).

[82] S. Serkez, O. Gorobtsov, D. E. Rivas, M. Meyer, B. Sobko, N. Gerasimova, N. Kujala, and G. Geloni, Wigner distribution of self-amplified spontaneous emission free-electron laser pulses and extracting its autocorrelation, Journal of Synchrotron Radiation **28**, 3 (2021).

[83] T. Weber, O. Jagutzki, M. Hattass, A. Staudte, A. Nauert, L. Schmidt, M. Prior, A. Landers, A. Bräuning-Demian, H. Bräuning, et al., K-shell photoionization of CO and $N_2$: is there a link between the photoelectron angular distribution and the molecular decay dynamics?, Journal of Physics B: Atomic, Molecular and Optical Physics **34**, 3669 (2001).

[84] M. Lundqvist, D. Edvardsson, P. Baltzer, and B. Wannberg, Doppler-free kinetic energy release spectrum of $N_2^{2+}$, Journal of Physics B: Atomic, Molecular and Optical Physics **29**, 1489 (1996).

[85] M. J. Frisch, G. W. Trucks, H. B. Schlegel, G. E. Scuseria, M. A. Robb, J. R. Cheeseman, G. Scalmani, V. Barone, B. Mennucci, G. A. Petersson, H. Nakatsuji, M. Caricato, X. Li, H. P. Hratchian, A. F. Izmaylov, J. Bloino, G. Zheng, J. L. Sonnenberg, M. Hada, M. Ehara, K. Toyota, R. Fukuda, J. Hasegawa, M. Ishida, T. Nakajima, Y. Honda, O. Kitao, H. Nakai, T. Vreven, J. A. Montgomery, Jr., J. E. Peralta, F. Ogliaro, M. Bearpark, J. J. Heyd, E. Brothers, K. N. Kudin, V. N. Staroverov, R. Kobayashi, J. Normand, K. Raghavachari, A. Rendell, J. C. Burant, S. S. Iyengar, J. Tomasi, M. Cossi, N. Rega, J. M. Millam, M. Klene, J. E. Knox, J. B. Cross, V. Bakken, C. Adamo, J. Jaramillo, R. Gomperts, R. E. Stratmann, O. Yazyev, A. J. Austin, R. Cammi, C. Pomelli, J. W. Ochterski, R. L. Martin, K. Morokuma, V. G. Zakrzewski, G. A. Voth, P. Salvador, J. J. Dannenberg, S. Dapprich, A. D. Daniels, Farkas, J. B. Foresman, J. V. Ortiz, J. Cioslowski, and D. J. Fox, Gaussian09, Gaussian Inc. Wallingford CT 2009.

[86] M. Barbatti, M. Bondanza, R. Crespo-Otero, B. Demoulin, P. O. Dral, G. Granucci, F. Kossoski, H. Lischka, B. Mennucci, S. Mukherjee, et al., Newton-X platform: New software developments for surface hopping and nuclear ensembles, Journal of Chemical Theory and Computation **18**, 6851 (2022).

[87] J. C. Tully, Molecular dynamics with electronic transitions, The Journal of Chemical Physics **93**, 1061 (1990).

[88] S. Mai, P. Marquetand, and L. González, Nonadiabatic dynamics: The SHARC approach, Wiley Interdisciplinary Reviews: Computational Molecular Science **8**, e1370 (2018).

[89] H.-J. Werner, P. J. Knowles, G. Knizia, F. R. Manby, and M. Schütz, Molpro: a general-purpose quantum chemistry program package, Wiley Interdisciplinary Reviews: Computational Molecular Science **2**, 242 (2012).

[90] H.-J. Werner, P. J. Knowles, F. R. Manby, J. A. Black, K. Doll, A. Heßelmann, D. Kats, A. Köhn, T. Korona, D. A. Kreplin, et al., The molpro quantum chemistry package, The Journal of Chemical Physics **152**, 144107 (2020).

[91] S. Seritan, C. Bannwarth, B. S. Fales, E. G. Hohenstein, S. I. Kokkila-Schumacher, N. Luehr, J. W. Snyder, C. Song, A. V. Titov, I. S. Ufimtsev, et al., Terachem: Accelerating electronic structure and ab initio molecular dynamics with graphical processing units, The Journal of Chemical Physics **152**, 224110 (2020).

[92] S. Seritan, C. Bannwarth, B. S. Fales, E. G. Hohenstein, C. M. Isborn, S. I. Kokkila-Schumacher, X. Li, F. Liu, N. Luehr, J. W. Snyder Jr, et al., Terachem: A graphical processing unit-accelerated electronic structure package for large-scale ab initio molecular dynamics, Wiley Interdisciplinary Reviews: Computational Molecular Science **11**, e1494 (2021).

[93] Data recorded for the experiment at the European XFEL are available at https://doi.org/10.22003/xfel.eu-data-002979-00.